DISLOCATION TRANSPORT OF OXYGEN

DURING FATIGUE CRACK GROWTH.

by

JOHN WALLACE/SWANSON/ B.S.E.M.

AFIT-CI-75-6

THESIS

Presented to the Faculty of the Graduate School of

The University of Texas at Austin

in Partial Fulfillment

of the Requirements

for the Degree of

MASTER OF SCIENCE IN ENGINEERING

THE UNIVERSITY OF TEXAS AT AUSTIN

May 1977

REPORT DOCUMENTATION PAGE		READ INSTRUCTIONS BEFORE COMPLETING FORM
1 REPORT NUMBER CI 78-6	2 GOVT ACCESSION NO.	3 RECIPIENT'S CATALOG NUMBER
4 TITLE (and Subtitle) Dislocation Transport of Oxygen During Fatigue Crack Growth		5 TYPE OF REPORT & PERIOD COVERED Thesis
		6 PERFORMING ORG. REPORT NUMBER
7 AUTHOR(s) Capt John W. Swanson		8 CONTRACT OR GRANT NUMBER(s)
9 PERFORMING ORGANIZATION NAME AND ADDRESS AFIT Student at the University of Texas, Austin TX		10 PROGRAM ELEMENT, PROJECT, TASK AREA & WORK UNIT NUMBERS
11 CONTROLLING OFFICE NAME AND ADDRESS AFIT/CI WPAFB OH 45433		12 REPORT DATE May 1977
		13 NUMBER OF PAGES 43 Pages
14 MONITORING AGENCY NAME & ADDRESS(if different from Controlling Office)		15 SECURITY CLASS. (of this report) Unclassified
		15a DECLASSIFICATION/DOWNGRADING SCHEDULE

16 DISTRIBUTION STATEMENT (of this Report)

Approved for Public Release; Distribution Unlimited

17. DISTRIBUTION STATEMENT (of the abstract entered in Block 20, if different from Report)

18 SUPPLEMENTARY NOTES

APPROVED FOR PUBLIC RELEASE AFR 190-17.

JERRAL F. GUESS, Captain, USAF
Director of Information, AFIT

19 KEY WORDS (Continue on reverse side if necessary and identify by block number)

20. ABSTRACT (Continue on reverse side if necessary and identify by block number)

DISLOCATION TRANSPORT OF OXYGEN

DURING FATIGUE CRACK GROWTH

APPROVED:

ACKNOWLEDGMENTS

John Wallace Swanson

The University of Texas

Austin, Texas

April, 1977

iii

ABSTRACT

The effect of an oxygen environment on fatigue crack growth of Monel 404, commercially pure titanium, 2219-T87 and 7075-T651 aluminum alloys was investigated. Use of Auger Electron Spectroscopy and Secondary Ion Mass Spectroscopy indicated transport of the oxygen environment into the metal matrix coincident with passage of the fatigue crack. This evidence supports the theory of dislocation sweep-in of gaseous environments in the form of Cottrell atmospheres about the dislocations. For all materials tested, oxygen was shown to be transported during fatigue crack growth an estimated 125 to 600 Å deeper into the matrix than that observed strictly by diffusion. An increase in the growth rate for an oxygen environment compared to that in vacuum was observed for Monel 404 and titanium by a factor of approximately 5 and 2, respectively. Little increase in growth rate was apparent for the aluminum alloys. The increased growth rate can be explained as a result of reduced or modified plasticity in the matrix ahead of the crack tip due to the oxygen swept in. The change in local plastic behavior can lead to a smaller residual strain zone in the wake of the crack, reducing the portion of the cycle during which the crack closes on itself. The effective ΔK consequently increases and crack growth rate necessarily increases.

TABLE OF CONTENTS

LIST OF TABLES

LIST OF FIGURES

C H A P T E R   I

INTRODUCTION

As industrial and scientific technology advances,
there is an ever increasing demand on the materials
scientist to develop more specialized and improved
structural materials. While developing new materials, he
also attempts to optimize use of presently available
materials by characterizing the nature of failures in
these materials, their response to types of loading, and
their response to various environments. Through such
studies, he is able to promote effective materials
selection, improving structure lifetime and dependability.

One area of considerable interest, particularly
to the aerospace industry, is crack propagation under
cyclic loading and environmental effects on the fatigue
crack growth rate, The materials dilemma is epitomized
in aircraft design, where weight and cost must be minimized
but dependability and performance must be maximized. These
clearly contradictory requirements can only be achieved if
full knowledge of material response is known. The loading
spectra of aircraft is such that fatigue damage is of
primary concern and design must thus include consideration
of environmental effects on fatigue crack growth rates.

1

Historically, design for fatigue damage has centered around statistical S/N data, where N is the number of cycles to failure and S is the cyclic loading stress level. With the inception of fracture mechanics theories, the S/N criteria is being replaced by da/dN, the crack growth per cycle, versus ΔK, the crack tip stress intensity range, combined with the fracture toughness of the material, K_C or K_{IC}. The mode one stress intensity factor K_I is a function of the remotely applied load P, the crack length, a, and a geometry factor Y. For a compact tension specimen the relation can be expressed as [1]:

$$K_I = YPa^{1/2}/BW$$

where B is the thickness and W the width of the specimen. Geometric factors have been calculated for various dimensions of compact tension specimens. For fatigue tests, where the loading is cyclic, the range in stress intensity, ΔK, is determined from the above equation by substituting ΔP for P. Maintaining ΔP constant during a test, ΔK increases with crack length so growth rate is constantly increasing until the inherent fracture toughness of the material is reached. The plane strain fracture toughness, K_{IC}, is the K level at which unstable,

rapid crack growth occurs leading to failure of the component. The designer makes use of such data by assuming the presence of a flaw or crack of length determinable by nondestructive techniques and calculating the stress intensity. From the test data he then determines fatigue crack growth rate as a function of expected loading history and arrives at a good estimate of structure lifetime.

For experimental evaluation of environmental effects on crack growth, a desirable approach is to maintain a constant ΔK, which should give a constant amount of damage in the front of the crack. An observed change in da/dN upon introduction of a new environment is then indicative of the environmental influence. The general effect of a gaseous environment such as water vapor, oxygen or hydrogen is to increase fatigue crack growth rate above that which occurs in the baseline inert gas or vacuum environment [2,3]. This "embrittling" nature of the environment may arise through an alteration of bonding strength at the crack tip resulting in premature decohesion.

Another possibility is that the environment is transported into the metal matrix ahead of the crack tip, decreasing or modifying the local plastic behavior of the matrix in this region, thus changing the crack closure

load in the crack closure model of Elber [4,5]. The crack closure concept consists of the well-documented fact that during part of the loading cycle, the crack closes due to a residual displacement pattern in the wake of the crack. This residual displacement arises from surface roughness and volume change due to the deformation. The resulting crack closure leads to loss of the singularity associated with the crack and the definition of an effective range in stress intensity, ΔK_{eff}, which is calculated from the load range during which the crack remains open. The change in plastic behavior results in a smaller residual displacement in the wake of the crack, increasing the effective ΔK and consequently increasing the growth rate.

The plasticity argument above depends on transport of the environment into the matrix to a much greater depth than diffusion would accomodate. A model for interstitial dislocation sweep-in has been proposed and applied to hydrogen [6,7], which indicates the plausibility of such transport, at least for a small atom like hydrogen. It is envisioned that since the region ahead of the crack tip is highly plastically deformed, with considerable dislocation production and motion, the environmental gases which adsorb and dissociate at the crack tip are picked up by dislocations as "Cottrell atmospheres" [8]. The

dislocations then carry the dissociated gases into the
matrix until the atmosphere is stripped from the dislo-
cation, or the dislocation becomes immobilized. Inherent
to this transport model is reduction in plasticity ahead
of the crack tip due to the drag force exerted on the
moving dislocations by the solute atoms being swept along
with them [9].

Problems arise, however, in an attempt to apply
the mathematical model of transport to a larger atom,
such as oxygen. The maximum penetration distance by
dislocation transport based on the Tien, et. al., model [7]
is given by:

$$X = \frac{DE}{kT(30b)2f}$$

where D is diffusivity of the hydrogen in the lattice,
E the dislocation/solute binding energy, 30 Burger's
vectors the estimated hydrogen/dislocation interaction
distance, and f the fatigue frequency. For oxygen, the
binding energy is estimated to be 0.5 eV [10] and the
interaction distance approximately 3 Burger's vectors.
Using the above equation, for sweep-in of 100 to 1000
angstroms at room temperature and a cyclic frequency of
1 Hz, the oxygen diffusivity would have to be approximately
10^{-15} to 10^{-14} cm^2/sec. Since diffusivity data for

oxygen in metals at room temperature indicates diffusivities more on the order of 10^{-20} cm^2/sec, sweep-in of oxygen by this model using the lattice diffusivity would be negligible. The diffusion rate near the surface could be enhanced by the less constrained configuration of this region, leading to faster diffusion of the interstitial oxygen. It is believed that oxygen may be transported into the matrix during the cyclic loading, offering an explanation of reported increased growth rate in an oxygen environment.

Since the sweep-in distance for dislocation transport of oxygen is expected to be extremely small, examination of this theory requires techniques which sample very thin surface layers, coupled with a means of etching the surface. These would provide a method of profiling oxygen concentration into a fatigue crack surface. A commonly employed method of gradual etching is inert ion sputtering, involving ionization of argon or other large inert gas atoms and accelerating these ions toward the surface of interest. Etching results from the ion/surface collisions, and the sputtered ions are mass analyzed with Secondary Ion Mass Spectroscopy (SIMS).

Another suitable surface technique is Auger Electron Spectroscopy (AES) which uses a focused electron

beam to excite atoms in the material under examination. In returning to their ground state, a percentage of the excited atoms undergo the Auger process which, simply stated, is the ejection of an outer shell electron having an energy directly related to the element involved [11]. This characteristic energy is maintained only if the electron avoids inelastic collisions in the matrix, leading to escape depths of unperturbated Auger electrons on the order of 5 to 20 $\overset{\circ}{A}$.

SIMS gives direct mass information about all atoms being removed from the surface and is capable of differentiating between isotopes such as the oxygen-16 and oxygen-18 used in this study. AES provides elemental analysis of that which remains on the surface in a region covered by a focused electron beam about 5 μm in diameter for this study, much smaller than the inert ion beam size of about 0.5 mm. The following sections describe experiments performed using these complementary techniques to determine if oxygen concentration in the metal matrix is in fact enhanced during growth of a fatigue crack.

C H A P T E R   II

EXPERIMENTAL PROCEDURE

Fatigue Crack Growth

Compact tension (CT) specimens of the geometry shown in Figure 1 were machined from as received plate stock. Materials tested were Monel 404*, commercially pure titanium, and aluminum 7075-T651 and 2219-T87 alloys. Nominal compositions of the materials tested and ΔK levels used are given in Table 1. Preliminary fatigue crack growth experiments were carried out in commercially pure oxygen as the test environment. The results were promising, however it was decided that use of an oxygen isotope might clarify the SIMS results by differentiating between oxygen transported during fatigue and that present from material manufacturing and recontamination during the experiments. The isotope oxygen-18 was obtained as 99.9% pure from Monsanto Corporation. The CT specimens were metallographically polished on one side in the region of crack propagation. Scribe marks were made on the polished surface at 0.16 cm intervals for visual measurement of crack length during cycling. Prior to installation in the test chamber, the specimens were

---

*Registered trademark, The International Nickel Company, Inc.

POLISHED REGION

2H

W

B
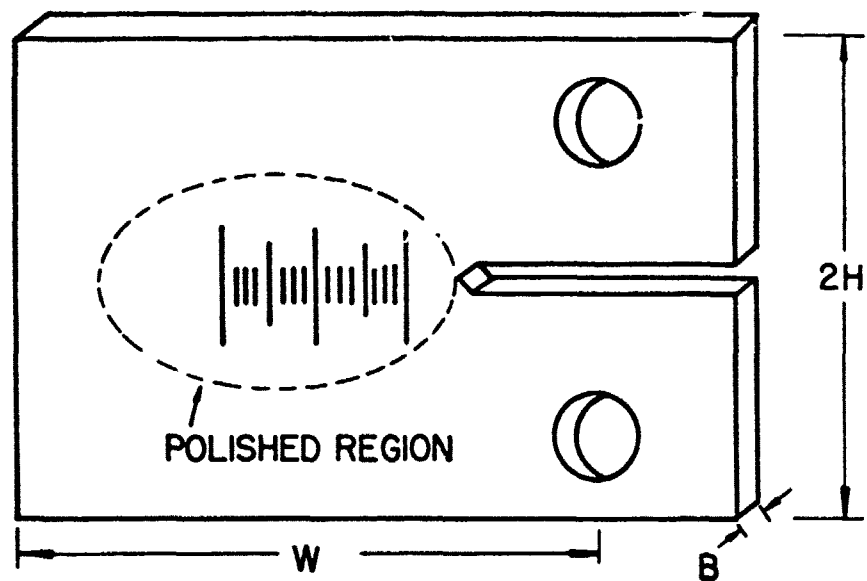
H = 3.175 cm

B = 0.635 cm

W = 7.938 cm

FIG. I   COMPACT TENSION SPECIMEN GEOMETRY

TABLE 1

Material Compositions and Experimental ΔK Levels

Material	Composition (%)	ΔK (MPa$\sqrt{m}$)
Monel 404	52-57 Ni, 0.5 max. Fe, 0.1 max. Mn, 0.15 max. C, 0.024 max. S, 0.1 max. Si, 0.05 max. Al, bal. Cu	33
Titanium	Commercially pure, ASTM B-265 (Gr. 2), 99.2 Ti	22
Aluminum 7075-T651	5.6 Zn, 2.5 Mg, 1.6 Cu, 0.3 Cr, bal. Al	11
Aluminum 2219-T87	6.3 Cu, 0.3 Mn, 0.06 Ti, 0.1 V, 0.2 Zr, bal. Al	11

cleaned in acetone and methanol.

An all metal, bakeable, ion pumped vacuum system was assembled to accept the CT specimens. The system was installed in an MTS closed-loop electro-hydraulic test frame for fatigue cycling through metal bellows. Rough pumping was accomplished by two zeolite absorption pumps through a bakeable valve to the chamber. The same absorption pump was always used as the first rough pump to trap normally unpumpable gases through rapid volume flow carrying these gases into the pump, the pump then being quickly valved off to prevent back streaming of the gases which zeolite will not trap. This step brought the chamber pressure to the 50 to 100 micron range. The cleaner second absorption pump was then opened to the chamber to bring the pressure down to 10 microns or less, at which time it was valved off and the ion pumps were opened to the chamber. Bakeable valves also separated the bottled oxygen-18 and the two 8 l/sec ion pumps from the chamber. A 1.2 meter length of copper tubing between the valve on the oxygen bottle and the bakeable valve at the chamber provided a pre-chamber to control oxygen input to the chamber without a metered leak valve. The valve to the copper tubing was open during pumping and the tubing was heated to desorb gases, insuring transfer of pure oxygen-18 when needed.

Figure 2(a) shows a schematic of the pumping system, capable of pressures below 1.3 μPa(10^{-8} Torr). The actual assembly is pictured in Figure 2(b).

With the pressure below 1.3 mPa (10^{-5} Torr), the sample was cyclically loaded to initiate the crack at the starter notch and to grow the crack to a length of 2.54 cm from the load line, the beginning of the gauge section used. In the interest of time, the starter crack was begun using a higher ΔK than the experimental value. ΔK was reduced to the experimental level sufficiently early for the crack to grow well beyond the plastic zone created by the higher ΔK before reaching the gauge section. This was done to prevent overload retardation [12,13] of the crack at the beginning of the experiment.

To maintain ΔK constant, it was necessary to reduce the load as crack length increased. This load shedding was accomplished at crack length intervals of 0.16 cm which maintained ΔK within approximately 6% of the desired value. The method of load shedding resulted in a ΔK variation, giving rise to small retardation effects and consequently some scatter in crack growth rate data.

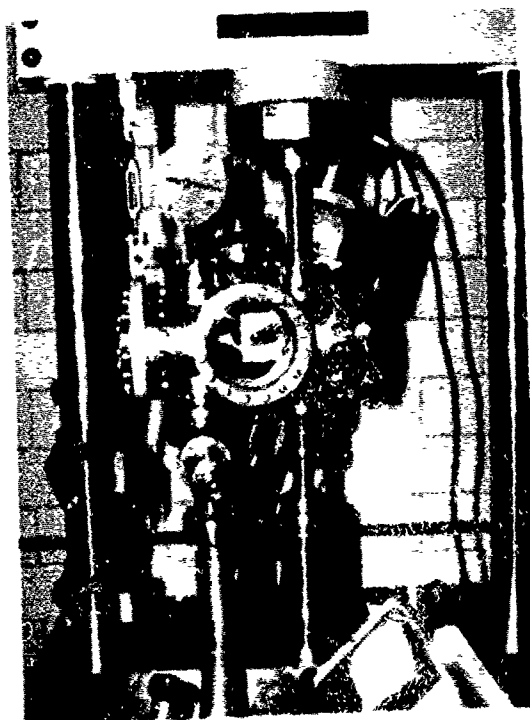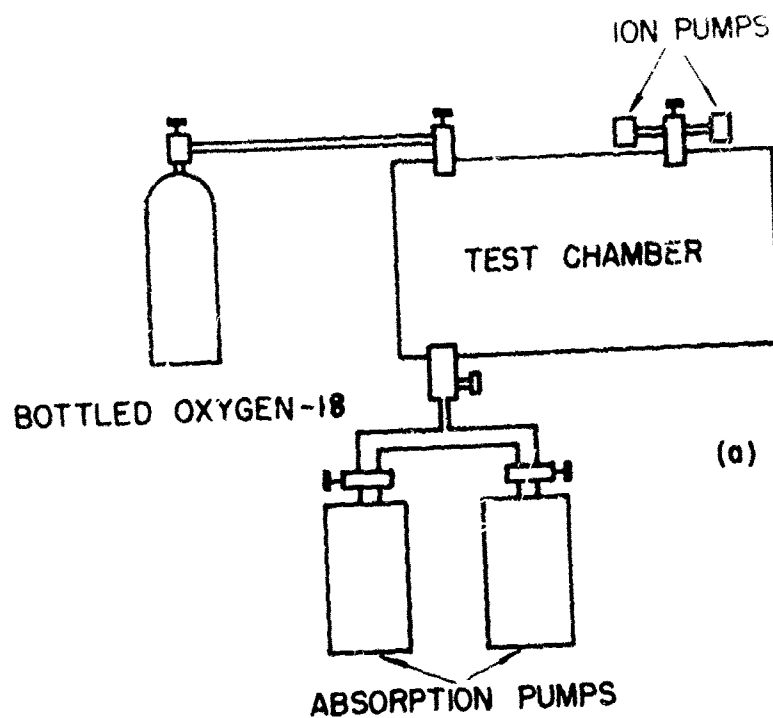After the chamber pressure had dropped below 13 μPa (10^{-7} Torr), the fatigue crack was extended 0.8 cm

FIG. 2 (a) SCHEMATIC DIAGRAM OF TEST CHAMBER PUMP SYSTEM.
(b) PICTORIAL OF CHAMBER AS INSTALLED IN FATIGUE TEST FRAME

by sinusoidal loading at a frequency of 10 sec^{-1}. Fatigue crack growth rate in vacuum was established during this extension by shedding load at each 0.16 cm scribe line and noting the number of cycles required to extend the crack to each line. The ion pumps were valved off and the oxygen isotope was introduced into the chamber to a pressure of 10 kPa (1 kPa for 2219 aluminum due to limited supply of the isotope). Cyclic frequency was reduced to 1 sec^{-1} and crack growth rate in oxygen at constant Δ was established through fatigue crack extension of 0.8 cm as before. Since growth rate in vacuum is independent of frequency in this frequency range, a higher frequency for vacuum could be used in the interest of time. It should also be noted that during crack extension in the isotope environment, the vacuum fatigue surface was exposed to the isotope but plastic deformation occurred in the vicinity of the crack tip and not along the surface formed in vacuum. This results in the fracture surface grown in vacuum being exposed to the isotope longer than the region fatigued in oxygen-18. In addition both regions were exposed to ambient oxygen the same time when transported to the AES/SIMS system.

Upon termination of the fatigue crack growth, the chamber was backfilled to atmospheric pressure with argon or nitrogen and the sample was removed. Segments of the

specimen were then cut for examination in the combined
AES/SIMS system. Their size was made compatible with the
system, such that each segment was from the fatigue crack
surface formed in either vacuum or the oxygen environment.
Cutting was done slowly with a hacksaw to prevent
enhanced diffusion through heating. The samples were
sealed in glass tubes evacuated to 0.13 mPa (10^{-6} Torr)
until AES/SIMS analysis was begun at the Physical
Electronics Laboratory in Eden Prairie, Minnesota.

Sample Analyses

Additional samples of Monel and titanium were
prepared by metallographically polishing through 0.05
micron diamond paste, then allowing them to oxidize in
ambient air. These samples were for examination of
roughness effects and to calibrate the ion sputtering
rates as described later. The polished and the fatigue
samples were ultrasonically cleaned in acetone and freon
and mounted in the AES/SIMS system. A sample of tantalum
with a Ta_2O_5 layer of thickness known to be 1000 Å was
also mounted. The system was not baked, to avoid
enhanced diffusion in the samples. Within a few hours
the chamber pressure was pumped to the 0.13 µPa
(10^{-9} Torr) range and analysis was begun. Argon was
backfilled to a pressure of 2.6 mPa (2 x 10^{-5} Torr) and

all electronic parameters were adjusted. An approximate
sputter rate calibration of 70 $\overset{o}{A}$ per minute was made by
noting the time necessary to sputter through the 1000 $\overset{o}{A}$
layer of Ta_2O_5.

The other samples were in turn rotated into
analysis position. The sputter-ion gun was turned on
simultaneously with the detectors and recorders, thus
producing simultaneous plots of AES oxygen signal and
negative SIMS mass 18 signal versus sputtering time.
AES signals for other elements and a range of SIMS
signals from mass 14 to 20 were monitored.

The fatigue samples were examined in a scanning
electron microscope and photographs were taken to observe
differences in fracture morphology for the two environ-
ments. A Bendix profilometer was used to obtain RMS
roughness measurements of the fracture surfaces.

C H A P T E R   III

RESULTS

Growth rate data from the fatigue experiments is
shown in Table 2. The factor of increased growth rate in
oxygen over that in vacuum is indicated by the ratio of
environmental growth rates. The aluminum alloys show
little increase in growth rates, while Monel and titanium
are very susceptible to increasing crack growth rates in
the oxygen environment.

Figures 3 through 10 depict the data from AES and
SIMS profiles, reduced as described later, to present the
information in clarified form. In each case, oxygen
concentration is extended deeper into the materials for
the fatigue crack propagated in an oxygen environment.
The profiles of the vacuum segments may be considered as
normal diffusion oxide profiles since no plastic defor-
mation occurred in this region during exposure to oxygen.
As noted before, oxygen was exposed a longer time to
the surface formed in the vacuum environment than that
formed in oxygen. The evidence suggests a thicker region
of enhanced oxygen level present for the samples where
the crack was grown in oxygen, which is consistent with
dislocation transport of oxygen during the plastic
deformation associated with the fatigue crack propagation.

17

TABLE 2

Crack Growth Rates and Ratio of Growth Rates

for Vacuum and Oxygen-18 Environments

Material	$da/dN|_{O^{18}} (\frac{\mu m}{cy})$	$da/dN|_{vac} (\frac{\mu m}{cy})$	Ratio
Monel 404	.423	.077	5.5
Titanium	.283	.152	1.9
Al 7075-T651	.140	.119	1.2
Al 2219-T87	.06₁	.054	1.1

Figure 3. AES Oxygen Profiles From Monel 404 Fatigue Crack Surfaces Formed in Vacuum and Oxygen-18 Environments.

Figure 4. SIMS Oxygen-18 Profiles From Monel 404 Fatigue Crack Surfaces Formed in Vacuum and Oxygen-18 Environments.

Figure 5. AES Oxygen Profiles From Titanium Fatigue Crack Surfaces Formed in Vacuum and Oxygen-18 Environments.

Figure 6. SIMS Oxygen-18 Profiles From Titanium Fatigue Crack Surfaces Formed in Vacuum and Oxygen-18 Environments.

Figure 7.   AES Oxygen Profiles From 2219 Aluminum Fatigue Crack
Surfaces Formed in Vacuum and Oxygen-18 Environments.

Figure 8. SIMS Oxygen-18 Profiles From 2219 Aluminum Fatigue Crack Surfaces Formed in Vacuum and Oxygen-18 Environments.
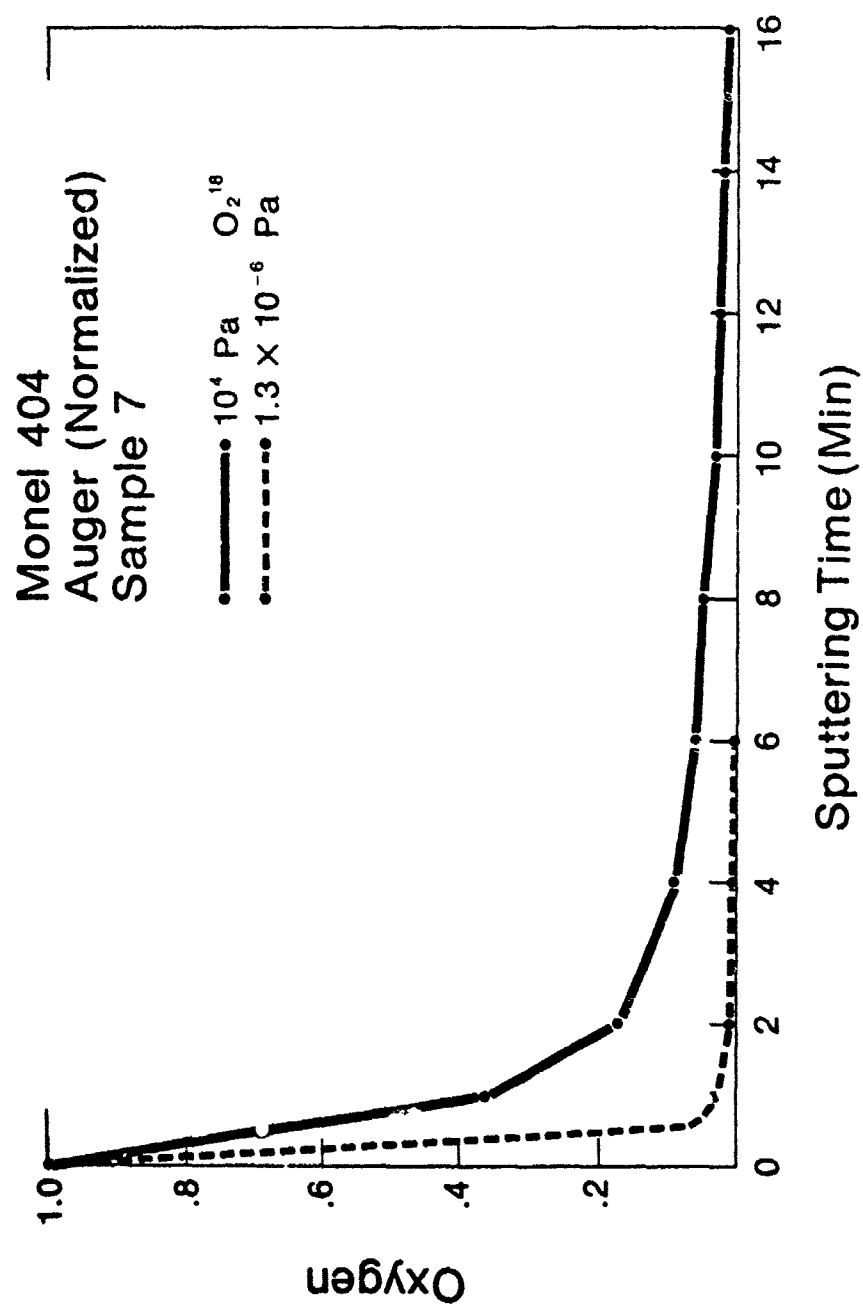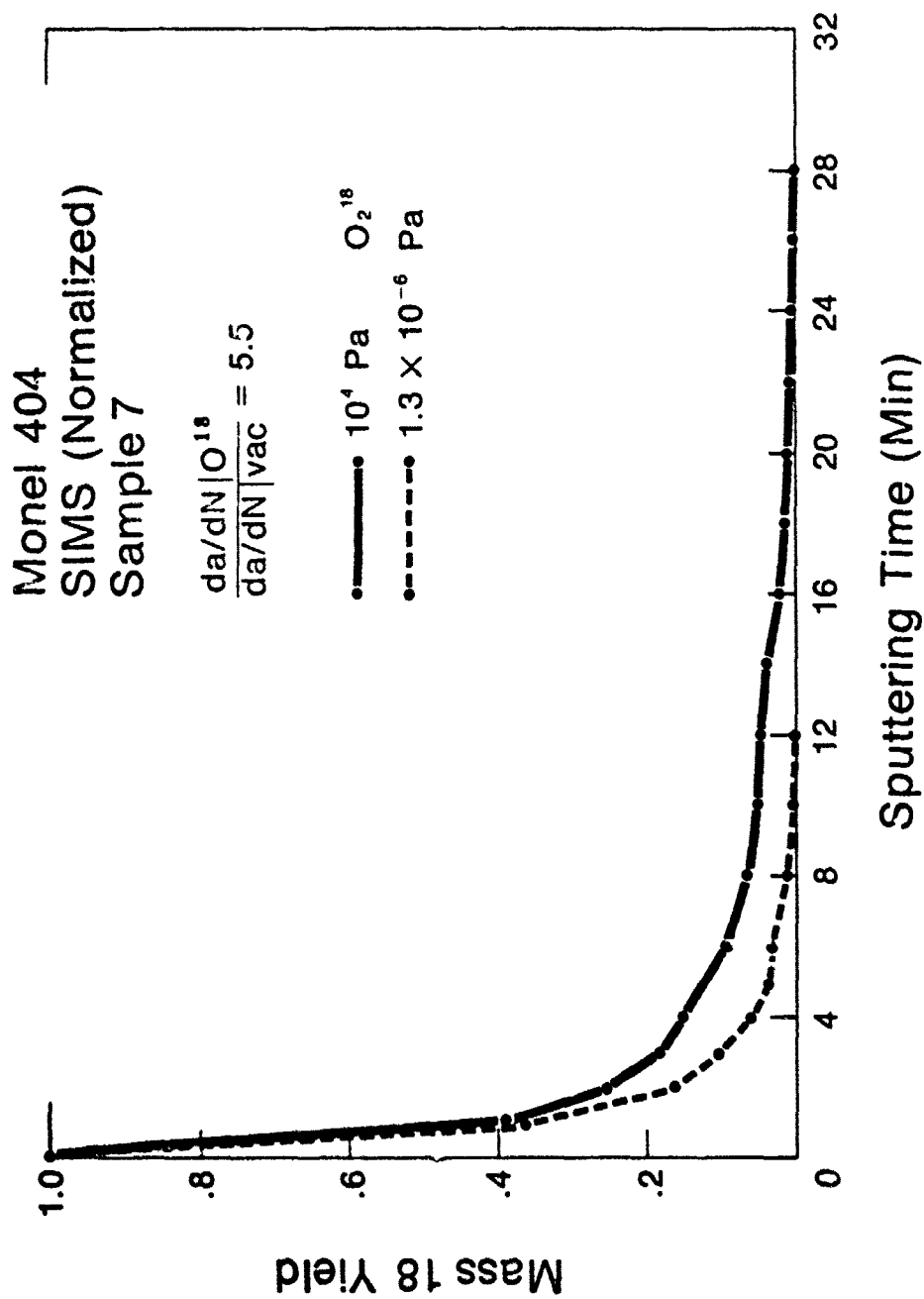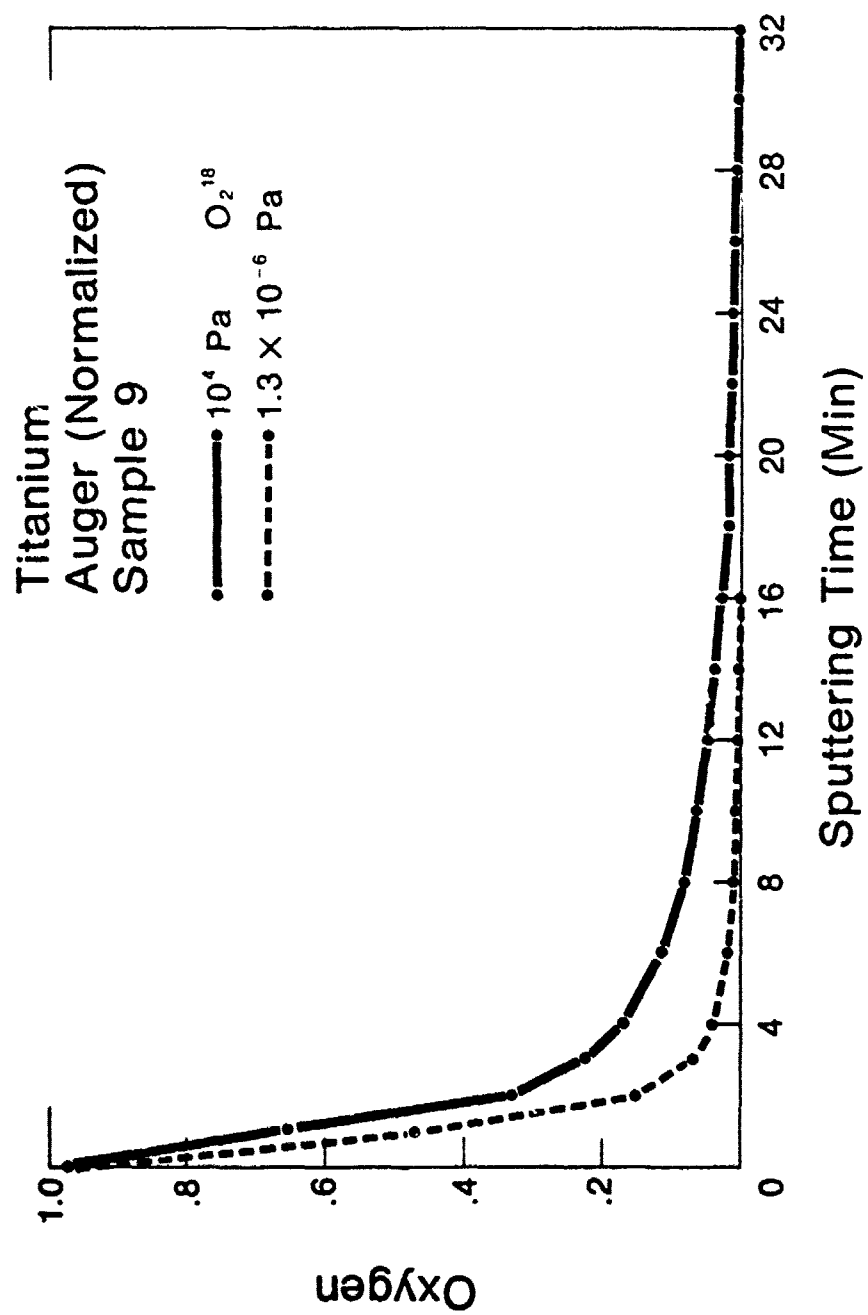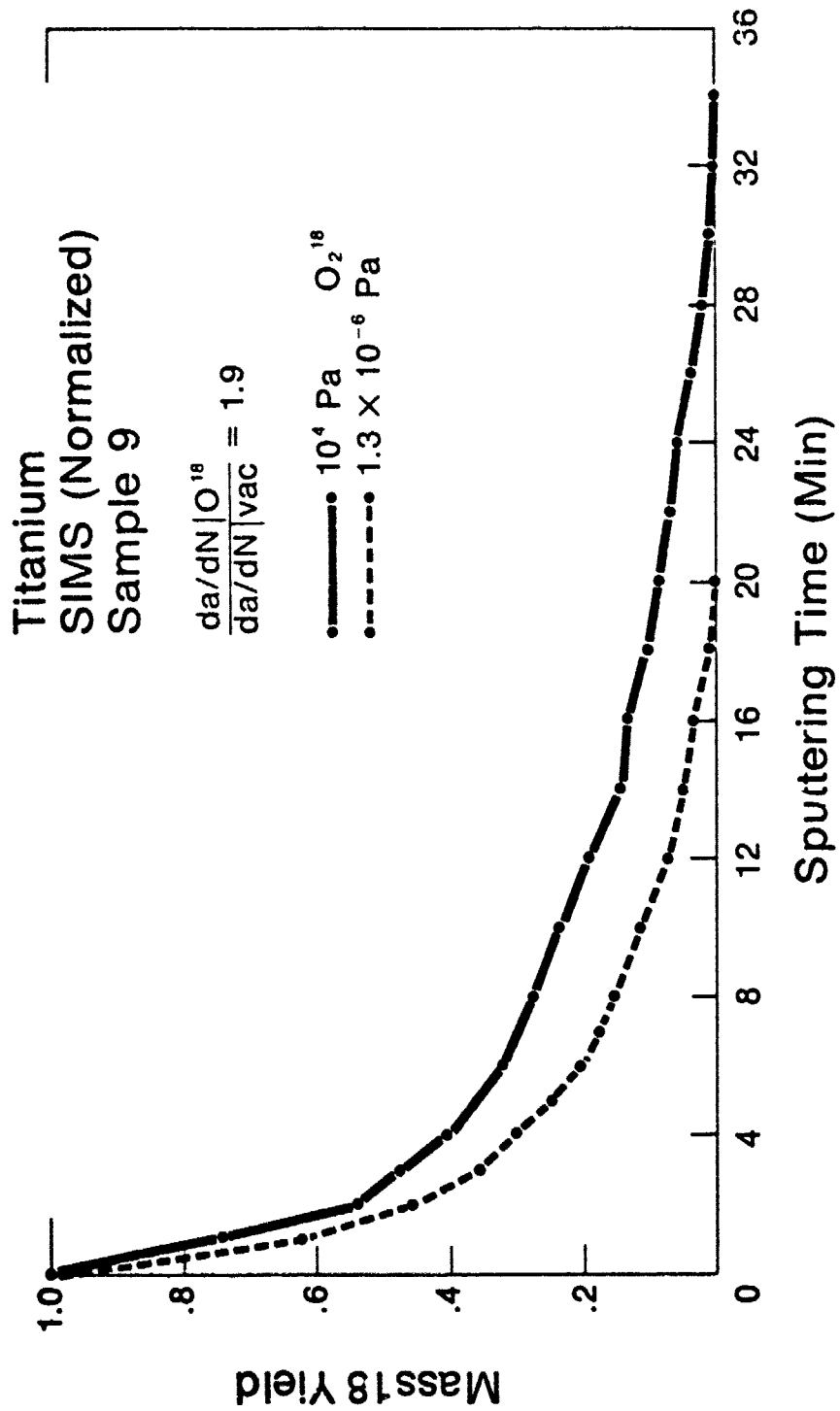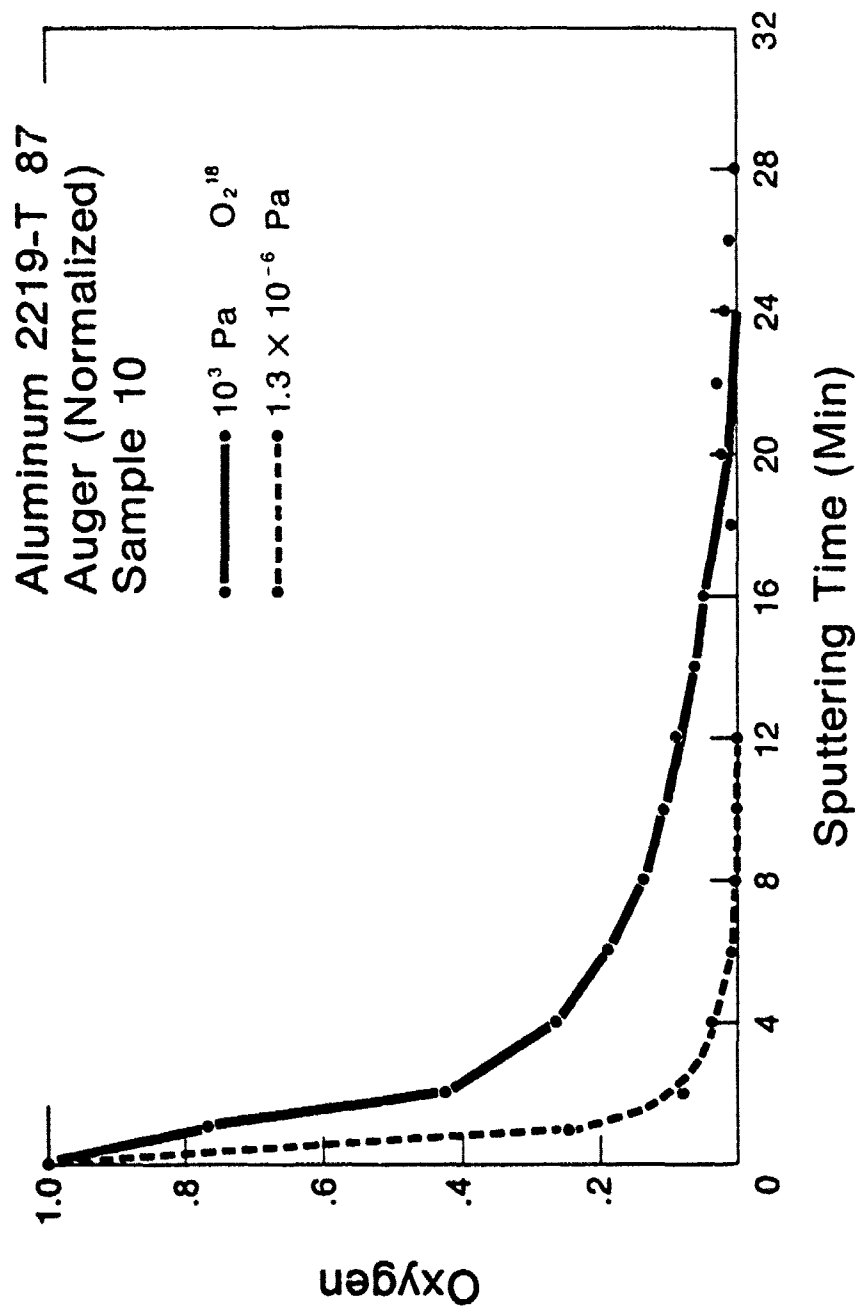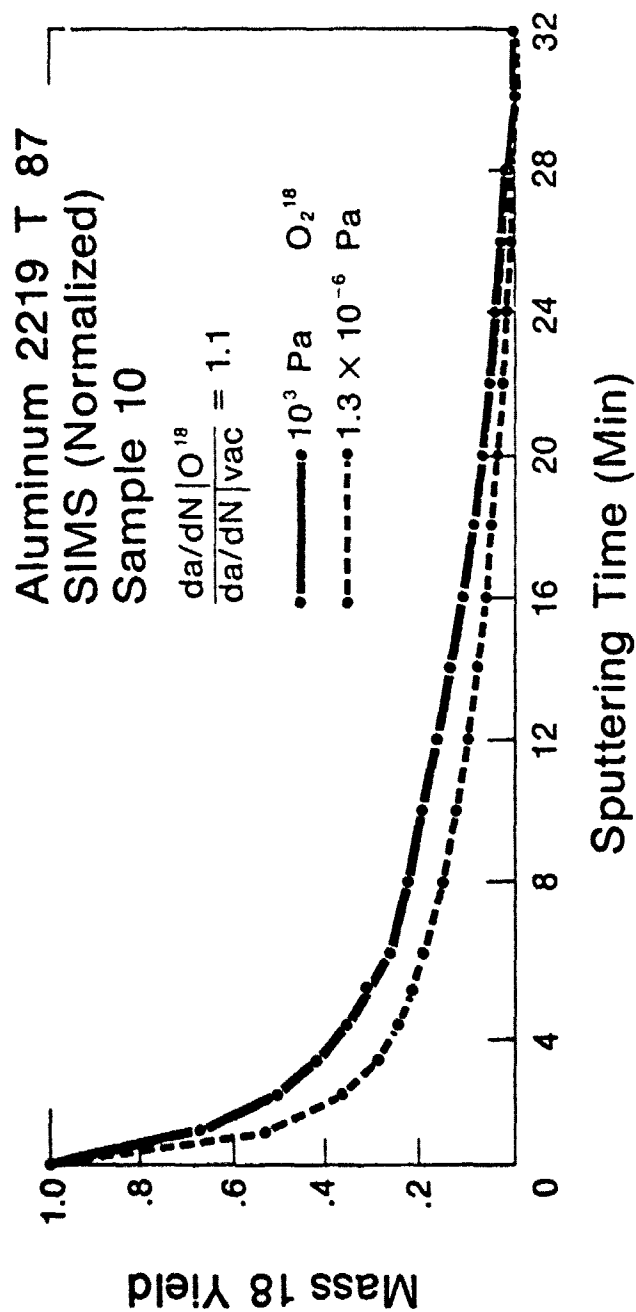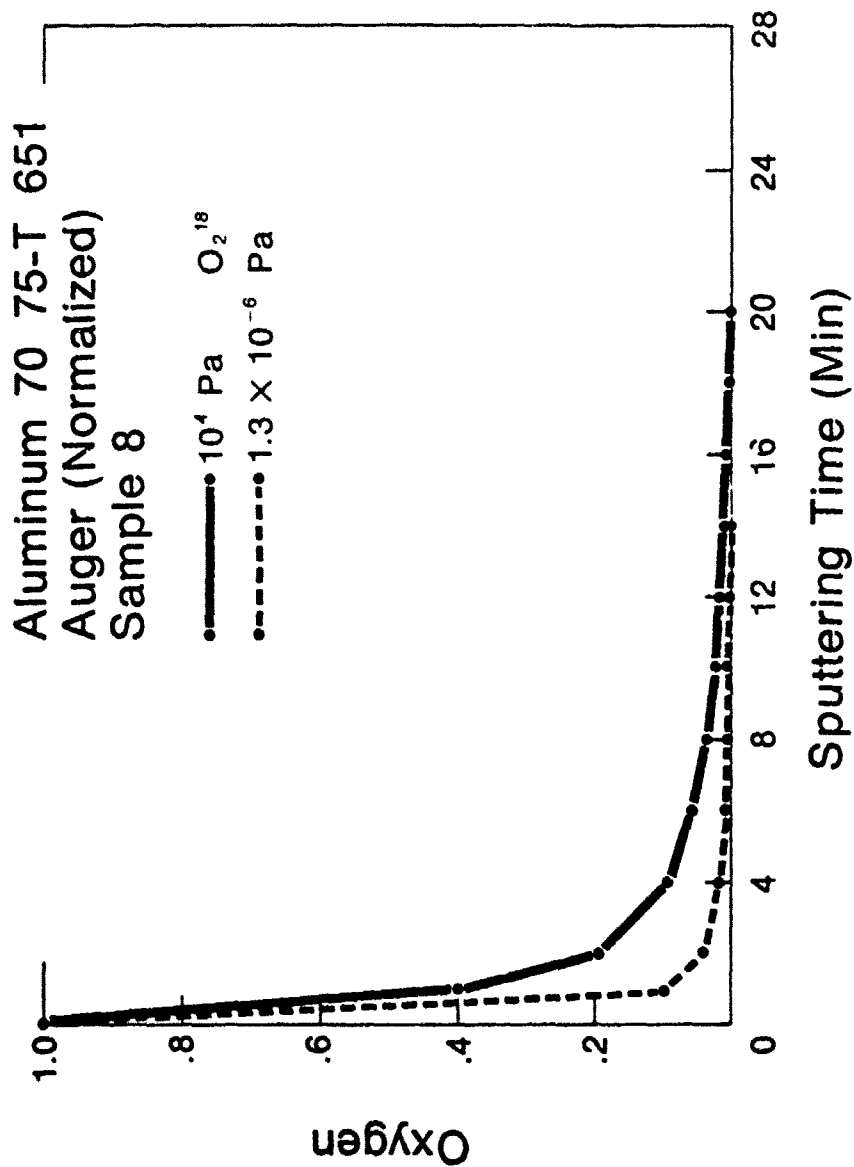
Figure 9. AES Oxygen Profiles From 7075 Aluminum Fatigue Crack Surfaces Formed in Vacuum and Oxygen-18 Environments.
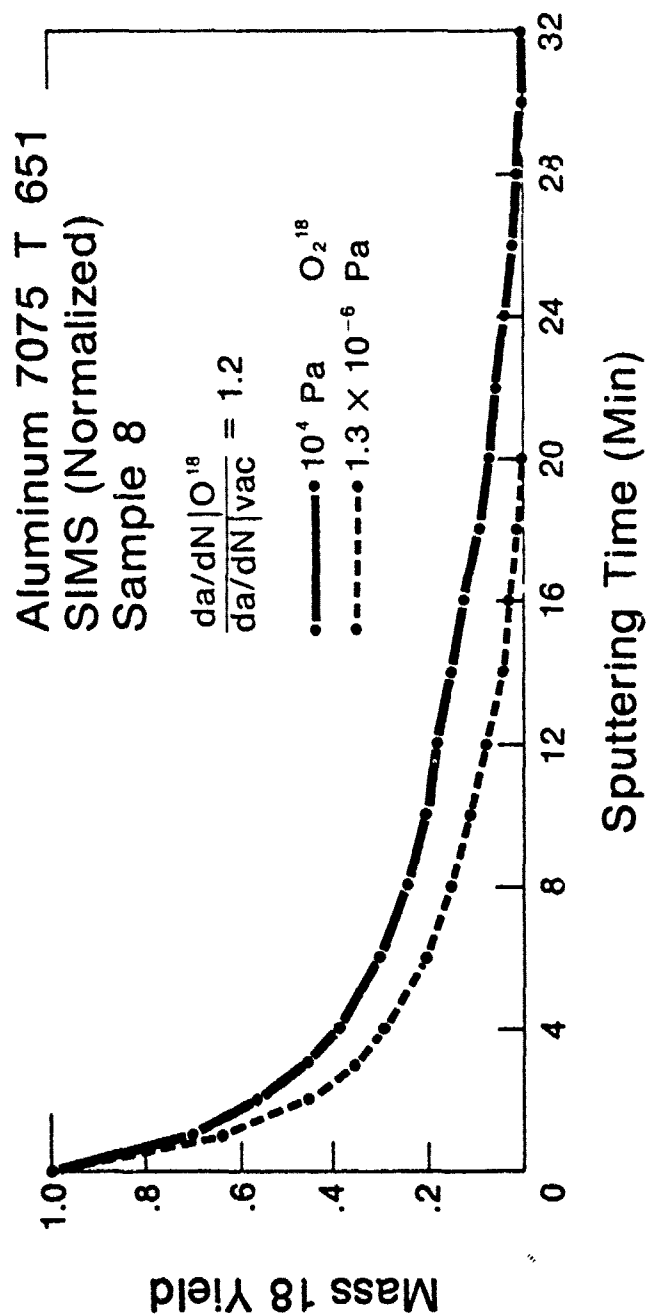
Figure 10. SIMS Oxygen-18 Profiles From 7075 Aluminum Fatigue Crack Surfaces Formed in Vacuum and Oxygen-18 Environments.

As can be seen from Table 3, roughness varied in some cases between samples of the same material for different environments. Due to non-colinearity of the ion beam with the SIMS and the AES optics, results of these techniques can be susceptible to sample roughness variations. For this reason as well as to attempt to get a directly comparable sputtering rate, samples of highly polished Monel and titanium were sputter profiled using identical ion beam parameters as for the fatigue samples. This treatment should produce the same profile as the vacuum fatigue samples, except for any roughness effects, since their normal diffusion controlled oxide thickness should be very close to that of the vacuum sample surfaces. The data showed point by point agreement between the polished and vacuum profiles, in spite of very large roughness differences. This is a strong indication that roughness effects on the data obtained must be minor at most. Since the time used to sputter the polished samples was known, sputter rate calibration could be made directly from the materials under study by determining the depth of the craters sputtered. This was planned, but the interferometer for measuring sputter depths did not become available.

Examination in a scanning electron microscope (SEM) permitted observation of fatigue crack morphology. For

TABLE 3

RMS Roughness of Fatigue Samples

Material	Environment	RMS Roughness (μ in)
Monel	vacuum	450
	oxygen-18	625
Titanium	vacuum	210
	oxygen-18	200
Al 7075-T651	vacuum	500
	oxygen-18	500
Al 2219-T87	vacuum	700
	oxygen-18	600-700

titanium and the aluminum alloys, no noticeable change in
deformation mode due to change in environment is observed
(Figures 11 - 13). In addition to the large increase in
roughness from earlier results, the Monel 404 surface
fatigued in oxygen showed a change in fracture appearance.
An indication at the fracture surface of an increase in
crystallographic deformation is apparent in Figures 14
and 15 for fatigue of Monel in oxygen, in agreement with
[2]. This is consistent with transport by a dislocation
mechanism which would be crystallographic in nature.
Figure 14(c) provides a comparison of grain size to the
fatigue surfaces of Figures 14(a) and (b), while Figure 15
shows comparisons of the two Monel fracture surfaces
at higher magnifications. The striations apparent in
Figure 15(d) have a width which is approximately the
nominal growth increment per cycle.

100 μm
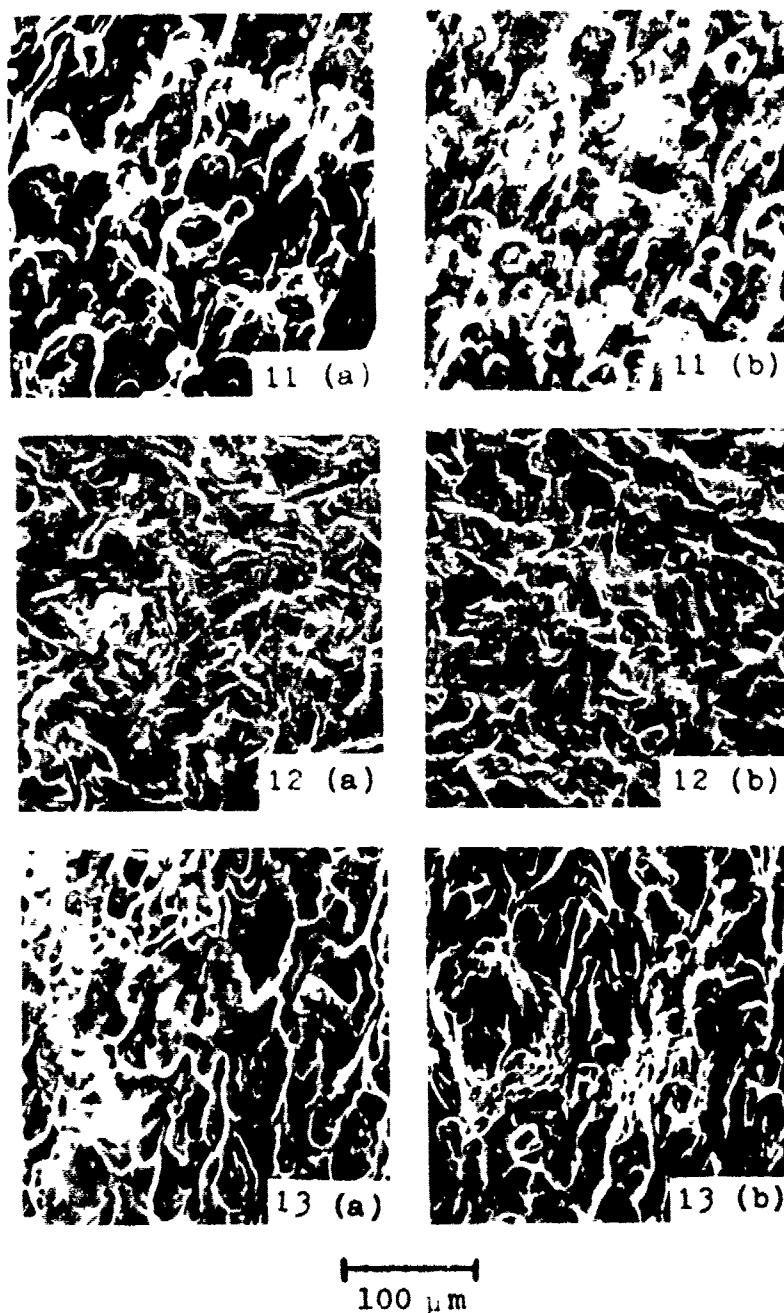
Scanning Electron Micrographs of Fatigue Crack Surfaces
Formed in (a) Vacuum and (b) Oxygen-18 Environment for:

Figure 11.   Aluminum 7075-T651

Figure 12.   Commercially pure Titanium

Figure 13.   Aluminum 2219-T87
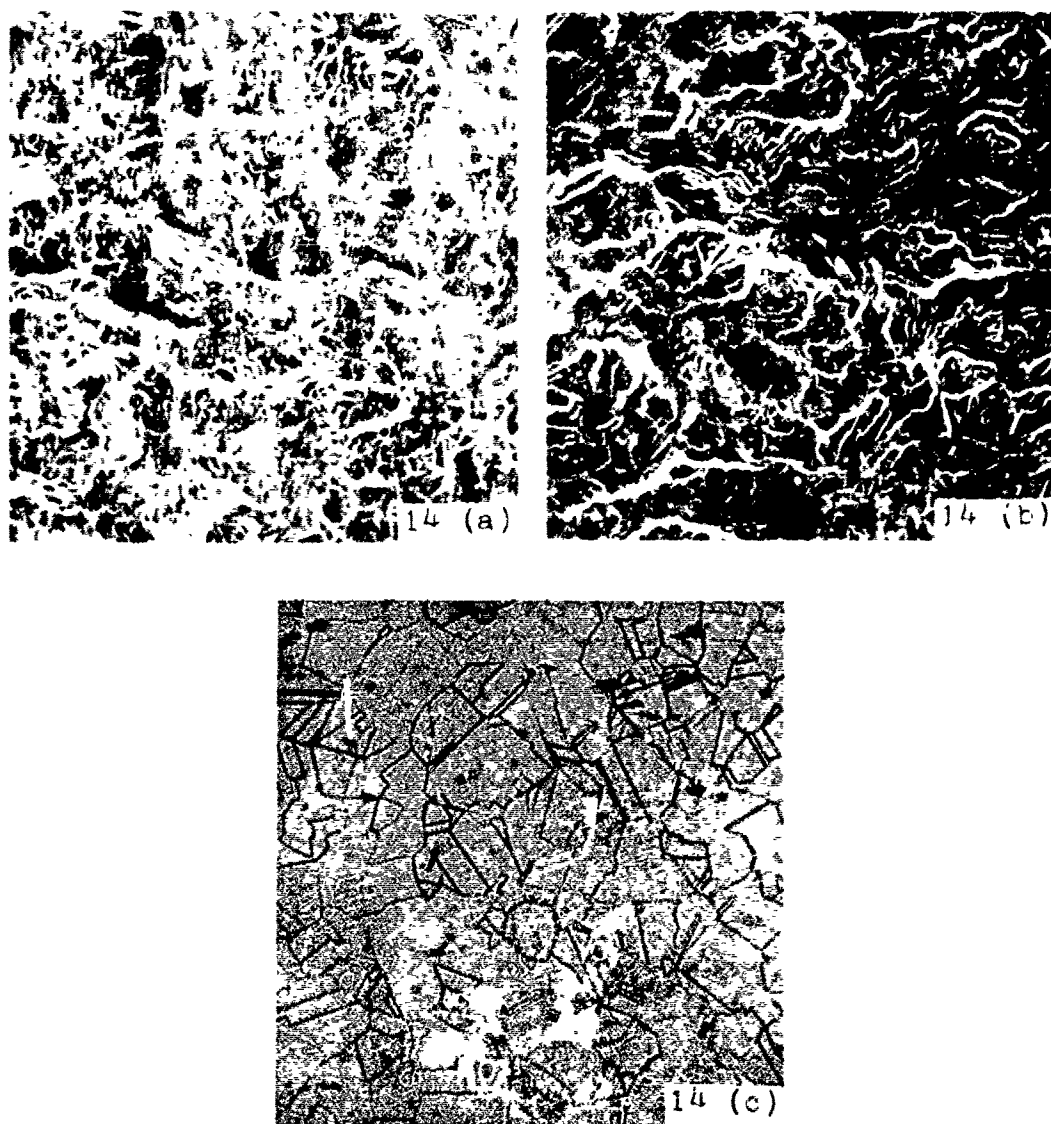
100 μm

Figure 14. Scanning Electron Micrographs of
Monel 404 Fatigue Surfaces Formed in (a)
vacuum and (b) Oxygen-18 Environment. Figure
14(c) Depicts Grain Structure at the Same
Magnification Through Optical Metallography
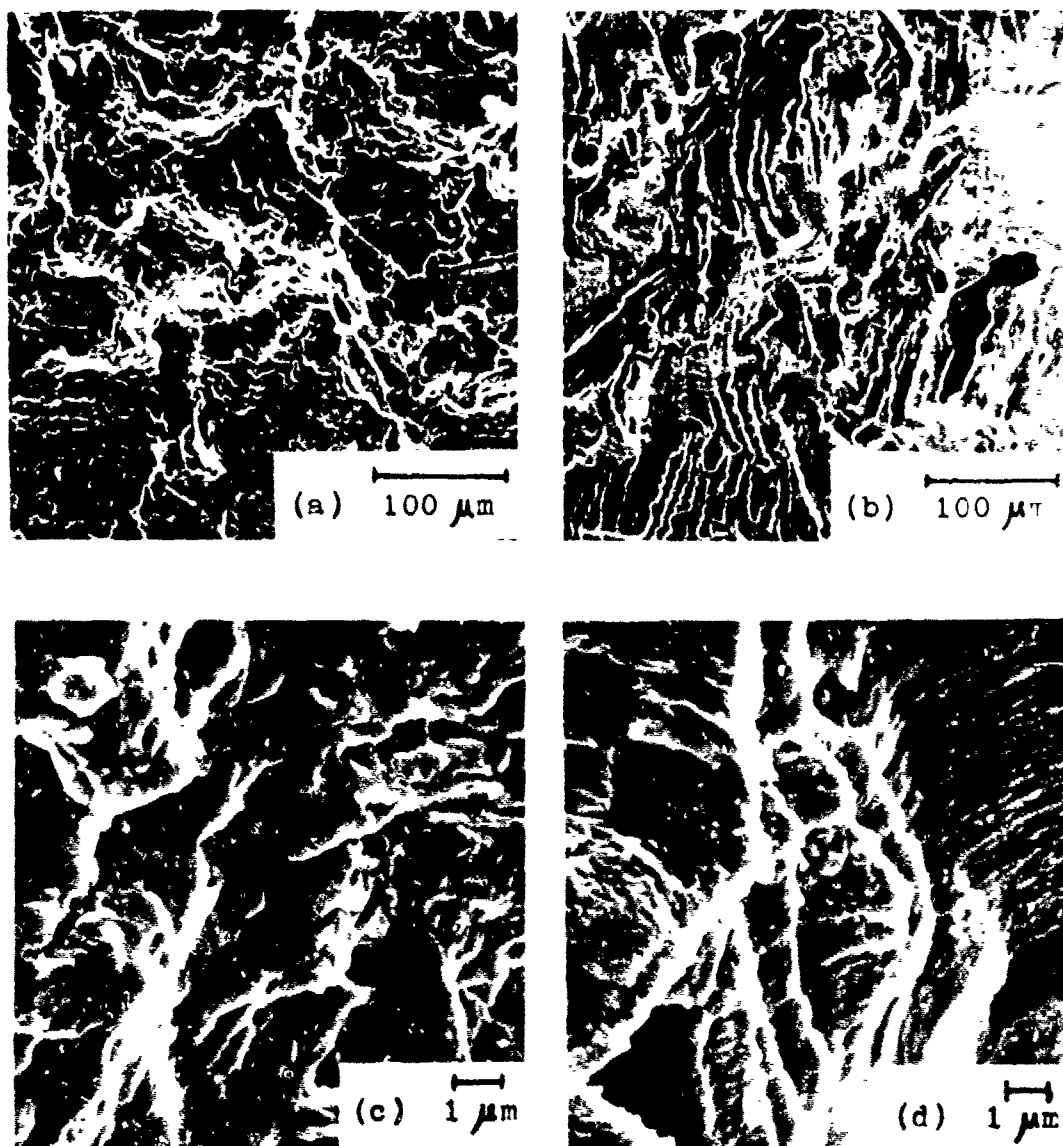
Figure 15. Scanning Electron Micrographs of
Increasing Magnification for Comparison of
Monel 404 Fatigue Surfaces Formed in (a), (c)
Vacuum and (b), (d) Oxygen-18 Environment.

CHAPTER IV

DISCUSSION

Choice of materials for this work was based primarily on oxidation characteristics and oxygen solubility. Since the oxygen transport is expected to be limited to the first few hundred angstroms of fatigue surface, a thick oxide would mask the effect. Monel had the advantage of slow oxidation, improving the chance of measurement of oxygen present due to dislocation transport. Titanium has an oxygen solubility much greater than the other materials tested, about 25 atomic % at room temperature [14]. It was anticipated that this increased solubility might enhance the transport mechanism and produce a more readily detectable indication of sweep-in. Aluminum forms a reasonably thin oxide and the alloys chosen are those of primary interest in on-going fatigue crack growth studies of aluminum alloys.

The raw AES/SIMS data was normalized to indicate oxygen level of one unit at the exterior fatigue crack surfaces. It was observed that the AES profiles leveled off at a value near zero, while the SIMS profiles continued to decrease with sputtering. The rate of decrease in the SIMS signal became very small after a reasonable period of sputtering. The continued gradual

decrease in SIMS signal is believed to be due to cratering of th_ ion beam and readsorption during sputtering. The point where the AES signal leveled and the SIMS signal had effectively leveled was noted and this signal magnitude was subtracted from the data as background.

There are consistent differences between the AES and SIMS depth profiles with the AES indicating a pro- portionately deeper enhanced oxygen level when compared to vacuum. Qualitatively, however, there are strong indications of transport in all cases. Sample roughness, residual gases and the shape of the sputtering crater may contribute to the shape of the profiles, the latter being particularly significant in the SIMS results.

One would expect oxidation and diffusion to result in a very sharp, well defined oxide layer followed by a steep oxygen gradient down to the material's solubility limit, particularly for the oxygen-18 since samples were exposed to the isotope only for the short duration of the fatigue tests. The AES profiles indicate such a gradient for oxygen in the vacuum samples, but the SIMS data indicates broadening, or a more gradual decrease in oxygen-13 with depth. For the samples fatigued in oxygen, dislocation transport could result in enhanced oxygen concentration, above the solubility limit, which would result in the observed more gradually decreasing

profile of oxygen. The well-defined oxide thickness is not present in either AES or SIMS profiles because the approximate sputter rate for the ion beam parameters used, as calibrated on Ta_2O_5, was 70 Å/min. At this rate the expected oxide would be removed very quickly and the profiles would not exhibit the flat surface oxide signal normally expected.

The steady state SIMS levels subtracted from the data were relatively high percentages of the overall signals, while the percentages subtracted from AES were near zero (Table 4). Part of this is due to the cratering effect of the ion beam where new oxide surface is constantly being removed by the low current density outer edges of the ion beam. This is observed only by the SIMS since it sees all of the atoms sputtered off of the surface. The higher spatial resolution AES is not influenced by this problem. It would be expected from the above argument that Monel with its thin oxide layer should be least affected by crater edge broadening in SIMS and it indeed has a low percentage level subtracted.

Readsorption would affect data from AES and SIMS but use of the isotope should reduce the effect for SIMS and the high sputter rate should minimize it for both techniques. It was observed that the background level could be increased by lowering the sputter rate, so

TABLE 4

Percentage of Maximum Signal

Subtracted from Data as Background

	AES		SIMS	
Material	Vacuum	Oxygen-18	Vacuum	Oxygen-18
Monel	3	10	4	5
Titanium	0	2	18	18
Al 7075-T651	0	37	8	38
Al 2219-T87	0	10	11	29

readsorption was indicated. Residual gases in the chamber during sputtering also contributed to the SIMS signal. It was expected that SIMS's excellent sensitivity in combination with the isotope would yield the best results, however the AES data appears to be less affected by broadening from readsorption, residual gases and crater edge effects.

The broadening problems combined with inaccurate sputter rate calibration prevent detailed quantitative analysis of depth of sweep-in. To estimate sweep-in distance relative to surface oxide thickness it was assumed that the vacuum profile approximates the oxide thickness. The point at which the profiles reach zero is experimentally uncertain so two approximations of oxide thickness were made by noting the sputtering time at which the oxygen signal from the samples fatigued in vacuum reduced to 0.1 and to zero. The same procedure was used on the data for samples fatigued in oxygen. The ratio of sputtering time on oxygen samples to that on vacuum samples should be approximately the same as the ratio of sweep-in depth to surface oxide thickness. An estimate of sweep-in depth can then be made by multiplying these ratios (Table 5) times the expected oxide thickness. As seen from Table 5, the SIMS data and AES data are self-consistent, but each indicates a different depth of

TABLE 5

Ratio of Sputtering Times from Sample Fatigued in Oxygen

to Sample Fatigued in Vacuum

at 0.1 of Maximum Level and at Background Sputtering Level

		Monel	Titanium	Al 2219	Al 7075
AES	Ratio of Sputtering Times for Signal = 0.1	6.3	2.7	5	3.8
	Ratio of Sputtering Times for Signal ≈ 0	5.4	2.5	3.7	3
SIMS	Ratio of Sputtering Times for Signal = 0.1	2	1.7	1.4	1.7
	Ratio of Sputtering Times for Signal ≈ 0	2.4	1.6	1	1.5

sweep-in for a given material. Using the AES ratios, which range from about 2.5 to 6, and an estimated oxide thickness of 50 to 100 angstroms, leads to the calculation of sweep-in depths on the order of 125 to 600 $\overset{\circ}{A}$.

The evidence of this research supports the theory of enhanced transport of oxygen, originating in the gaseous phase, into a metal matrix during fatigue crack propagation. The presently defined model for dislocation transport [7] does not explain the observed enhanced oxygen transport. The use of lattice diffusivity in the model may not be the appropriate value to use in computation of maximum distance of transport possible by dislocations since the lattice in the region of a free surface will be less constrained, which could lead to a higher diffusion rate. It seems unlikely that this could provide the necessary five or six orders of magnitude increase in diffusivity. Although the presently available models of dislocation transport do not explain the results, dislocation sweep-in still is the best candidate to explain the enhanced oxygen transport.

C H A P T E R   V

CONCLUSIONS

1. An increase in growth rate in an oxygen environment as compared to growth rate in vacuum is indicated for Monel 404 and commercially pure titanium. The increase is by a factor of approximately five for Monel and two for titanium. Little increase in growth rate is observed for aluminum 7075-T651 and 2219-T87 alloys.

2. Enhanced concentration of oxygen in the metal matrix due to propagation of a fatigue crack in an oxygen environment compared to a vacuum environment is indicated for Monel 404, commercially pure titanium, aluminum 7075-T651 and aluminum 2219-T87. This is consistent with a dislocation transport mechanism.

3. Comparison of metallurgically polished and fatigue crack surfaces formed in vacuum indicate that sample roughness contributed little error to the measurements.

4. Readsorption during sputtering, residual gases, and inaccurate sputter rate calibration prevent accurate determination of dislocation transport depths, but a rough estimate of 125 to 600 Å is made based on expected oxide thickness.

5. The fracture surfaces from oxygen and vacuum

40

environments appear the same for each material except
Monel 404. In this case fracture surface analysis shows
the deformation to have a crystallographic nature for
crack growth in the oxygen environment, again consistent
with the dislocation sweep-in model.

BIBLIOGRAPHY

1. Brown, William F., Jr., and Srawley, John E., Plane Strain Crack Toughness Testing of High Strength Metallic Materials, ASTM STP 410, pp. 14-15, American Society for Testing and Materials (1966).

2. Frandsen, J.D., Paton, N.E., and Marcus, H.L., "Met. Trans.," Vol. 5, pp. 1655-61 (1974).

3. Morris, W.L., Frandsen, J.D., and Marcus, H.L., ASTM STP 600, pp. 49-61, American Society for Testing and Materials (1976).

4. Elber, W., "Engineering Fracture Mech.," Vol. 2, p. 37 (1970).

5. Elber, W., in Damage Tolerance in Aircraft Structures, ASTM STP 486, p. 230, American Society for Testing and Materials (1971).

6. Fujita, F.E., in "Fracture of Solids," Interscience Publishers, New York (1963), p. 657.

7. Tien, J.K., Thompson, A.W., Bernstein, I.M., and Richards, R.I., "Met. Trans.," Vol. 7A, pp. 821-29 (1976).

8. Cottrell, A.H., Dislocations and Plastic Flow in Crystals, Chapter IV, Clarendon Press, Oxford (1953).

9. Ibid, p. 136.

10. Thompson, D.O., and Buck, O., in "Journal of Applied Physics," Vol. 38, No. 8, pp. 3057-3074 (1967).

11. Marcus, H.L., in "Journal of Metals," Vol. 29, No. 2, pp. 20-24 (1977).

12. Buck, O., Frandsen, J.D., and Marcus, H.L., "Spike Overload and Humidity Effects on Fatigue Crack Delay in Al 7075-T651," Fatigue Crack Growth Under Spectrum Loads, ASTM STP 595, pp. 101-112 (1976).

13. Hudson, C.M., and Hardrath, H.F., "Effects of Changing Stress Amplitude on the Rate of Fatigue Crack Propagation in Two Aluminum Alloys," NASA TN D-960 (1961).

14. Hawkins, D.T., Metals Handbook, 8th edition, Vol. 8, p. 327, American Society for Metals (1973).

VITA

John Wallace Swanson was born in Idaho Falls,
Idaho, on December 1, 1947, the son of Winifred and Herbert
Swanson. After completing his work at Uvalde High School,
Uvalde, Texas, in 1966, he studied for one year at The
University of Texas. He accepted an appointment to the
United States Air Force Academy, graduating from there in
1971 with a Bachelor of Science degree in engineering
mechanics. While serving as an officer in the Air Force,
he entered the graduate school of The University of
Texas in January, 1976.

Permanent address: 1651 Hamilton
                   Harlingen, Texas   78550

This thesis was typed by Sandy Stollenwerk.